

Storage ring studies on dissociative recombination and internal excitation of helium dimer ions

This article has been downloaded from IOPscience. Please scroll down to see the full text article.

2005 J. Phys.: Conf. Ser. 4 168

(<http://iopscience.iop.org/1742-6596/4/1/023>)

View [the table of contents for this issue](#), or go to the [journal homepage](#) for more

Download details:

IP Address: 38.107.179.210

The article was downloaded on 21/02/2012 at 16:36

Please note that [terms and conditions apply](#).

Storage ring studies on dissociative recombination and internal excitation of helium dimer ions

H B Pedersen,¹ H Buhr,¹ S Altevogt,¹ V Andrianarijaona,¹ H Kreckel,¹
L Lammich,¹ N de Ruelle,² E M Staicu-Casagrande,² D Schwalm,¹ D Strasser,³
X Urbain,² D Zajfman^{1,3} and A Wolf¹

¹ Max-Planck-Institut für Kernphysik, D-69117 Heidelberg, Germany

² Département de Physique, Université catholique de Louvain, B1348, Louvain-la-Neuve, Belgium

³ Department of Particle Physics, Weizmann Institute of Science, Rehovot, 76100, Israel

E-mail: henrik.pedersen@mpi-hd.mpg.de

Abstract. The dissociative recombination (DR) of the helium dimer ${}^3\text{He}^4\text{He}^+$ has been investigated at the heavy-ion Test Storage Ring (TSR) in Heidelberg at relative energies up to 40 eV. The vibrational level population in the stored ion beam was shown to be non-thermal with a fraction of 0.1–1% in higher vibrational states, resulting mainly from vibrational excitation in collisions with the residual gas species. The temporal evolution of the DR rate during storage showed evidence for an electron induced rotational de-excitation from the vibrational ground state. After characterizing the evolution of the rovibrational population of the stored ions, the zero energy DR rate coefficient was extracted from the measurement to be $\alpha_{\text{DR}}^{v=0}(0) = (7.3 \pm 2.1) \times 10^{-10} \text{ cm}^3/\text{s}$, and the DR reaction from the vibrational ground state was seen to proceed mainly to the $1s2s^1S$ and $1s2p^3P$ atomic limits. For $v \geq 3$, the DR reaction has a rate coefficient $\geq 2 \times 10^{-7} \text{ cm}^3/\text{s}$ and leads primarily to atomic fragments with $n \geq 3$. The energy dependent rate coefficient displays several prominent structures.

1. Introduction

The dissociative recombination (DR) of He_2^+ is of relevance both in models of the early universe [1], and in laboratory plasmas [2]. In particular, He_2^+ is the dominating ion at room temperature in the fundamental helium plasma for pressures above 5 mbar [2] and the role of DR in this plasma and afterglow has remained unclarified for decades. From a fundamental point of view the DR of He_2^+ attracts attention since the lowest vibrational level of He_2^+ has no favorable curve crossing with diabatic dissociative states of He_2 [3], and hence non-adiabatic couplings or other perturbative interactions should be expected to play an important role at low energies. For excited vibrational states ($v \geq 3$) favorable curve crossings do exist and the low-energy DR of the He_2^+ is therefore expected to be characterized by extreme variations of the cross sections among the low vibrational levels [3]. This is a challenge to the storage ring technique, since a good understanding of the ion beam evolution is mandatory to extract quantitative information from the measurements; in addition these properties offer unique opportunities to study vibrational cooling and heating processes during ion storage. A series of experiments has been performed at the TSR heavy-ion storage ring for both the infrared active isotopomer ${}^3\text{He}^4\text{He}^+$ [4] and the infrared inactive symmetric species ${}^4\text{He}_2^+$ [5]. Here we report results for ${}^3\text{He}^4\text{He}^+$, where the large variation in DR cross section was indeed used to explore both the ion beam evolution during storage as well as the DR process itself.

Due to the permanent dipole moment of ${}^3\text{He}^4\text{He}^+$ a rovibrational excitation in this ion originating from its creation process tends to decay by spontaneous emission during the ion storage. Radiative thermalization among the *vibrational* levels occurs on a characteristic time scale of only ~ 3 s [4]; after at most 10 s of storage, levels with $v \geq 3$ would be essentially unpopulated, giving no contribution to the DR signal despite the extreme rise [3] of the DR cross section with increasing vibrational quantum number. The *rotational* populations within the $v = 0$ level evolve over several tens of seconds under the influence of radiative transitions, and thermalization is reached after hundreds of seconds. In this work, these characteristic time scales are used to identify changes in vibrational or rotational populations. It should be emphasized that these relaxation time scales can only be shortened by the occurrence of additional processes, and should thus be considered as *maximum* times over which the vibrational and rotational level populations can evolve.

2. Experiment

The experiment was conducted at the Test Storage Ring (TSR) at the Max-Planck-Institut für Kernphysik in Heidelberg. Helium dimer ions were produced in a standard duoplasmatron ion source (pressure 0.4–1.1 mbar), accelerated to kinetic energies E_i of either 7.28 MeV or 3.36 MeV using an RF accelerator, and injected into the storage ring where they were stored at vacuum pressures of $5\text{--}10 \times 10^{-11}$ mbar for up to 70 s with a mean lifetime ($1/e$) of 9.8 s. The beam loss is mainly determined by ion collisions with species of the residual gas which is composed mostly ($\geq 90\%$) of H_2 . The TSR electron cooler [6,7] was used to apply phase space cooling to the stored He_2^+ ion beam for ~ 5 s after injection and to perform the electron-ion recombination experiments [8,9]. The difference between the average longitudinal ion and electron velocities defines the detuning velocity v_d and the corresponding detuning energy $E_d = (m/2)v_d^2$ (m denoting the electron mass). The collision velocities are distributed according to an anisotropic Maxwellian [8] characterized by the electron temperatures $kT_\perp = 10$ meV and $kT_\parallel = 0.5$ meV for the present experiment. At an ion energy of $E_i = 7.28$ MeV, the cooling energy of the electron beam (i.e., where $E_d = 0$) was $E_e^c = 571$ eV and electron densities n_e of 1.21×10^7 cm^{-3} and 5.5×10^6 cm^{-3} were used. At $E_i = 3.36$ MeV, the cooling energy was $E_e^c = 263$ eV and the electron density was 5.5×10^6 cm^{-3} . The stored ion beam was probed by Coulomb explosion imaging [10,11], and by DR measurements focusing on the rate coefficient [12] and on DR fragment imaging [9].

3. Rovibrational population of the stored ion beam and basic observations

3.1. Coulomb explosion imaging

The relative vibrational level populations of the stored ${}^3\text{He}^4\text{He}^+$ ions were monitored with Coulomb explosion imaging (CEI) of ions slowly extracted from the beam during storage [10,11]. Briefly, the distribution $P_v(\tilde{E}_k)$ of kinetic energy releases (\tilde{E}_k) following foil induced Coulomb explosion for an ensemble of ions in a given vibrational state v has a characteristic form [10] that reflects the distribution of nuclear positions and momenta in this state, and which can be modelled accurately [13]. For an ensemble of ions in several vibrational states the normalized kinetic energy distribution after Coulomb explosion

$$P(\tilde{E}_k, t) = \sum_v p_v(t) P_v(\tilde{E}_k) \quad (1)$$

is a superposition of the normalized distributions for the individual vibrational states, where the coefficients $p_v(t)$ represent the relative populations of the vibrational states v in the beam, and $\sum_v p_v(t) = 1$.

The measured kinetic energy distribution $P(\tilde{E}_k, t)$ at times 0–1 s indicates vibrational populations of $(56 \pm 3)\%$ in $v = 0$, $(13 \pm 4)\%$ in $v = 1$, $(16 \pm 5)\%$ in $v = 2$, and 15% distributed over the levels with $v \geq 3$. The distribution becomes narrower with storage time, and after 3 s no further change in its width was observed. This relaxed kinetic energy distribution ($t \geq 3$ s) without electron cooling compares very well with a Monte Carlo simulation for $P_{v=0}(\tilde{E}_k)$ [4]. Performing a least-squares fit to

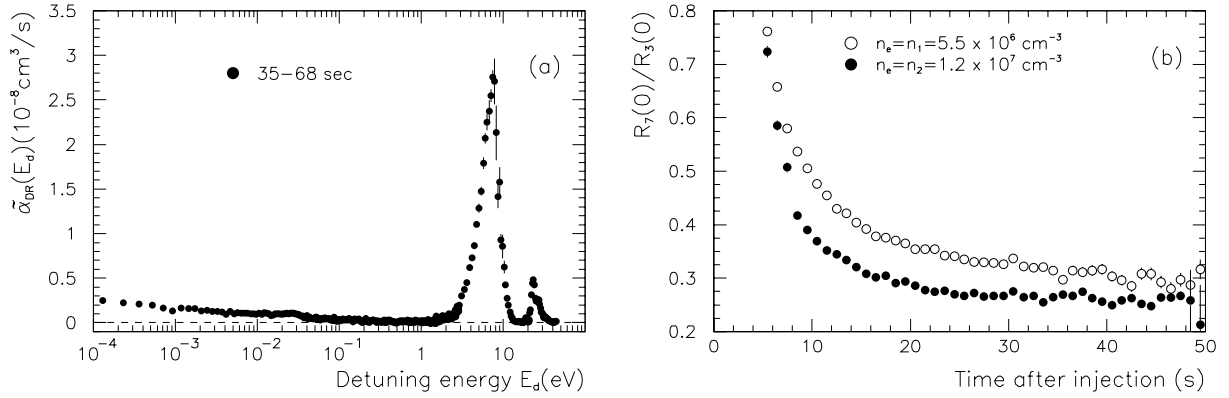


Figure 1. Absolute DR rate coefficients. (a) Toroid corrected DR rate coefficient over the full studied energy range. The overall accuracy of the $\tilde{\alpha}_{\text{DR}}$ scale is $\pm 15\%$. (b) DR rates $R_{(7)}(0;t)$ relative to the dissociative excitation rate $R_{(3)}(0;t)$, which is mostly determined by the residual gas pressure, as a function of time after injection as measured with the electron beam continuously on for electron densities of $n_e = n_1 = 5.5 \times 10^6 \text{ cm}^{-3}$ (open circles) and $n_e = n_2 = 1.2 \times 10^7 \text{ cm}^{-3}$ (filled circles). To compare the ratios $R_{(7)}(0;t)/R_{(3)}(0;t)$ at the two different electron densities the data set corresponding to n_1 has been scaled by a suitable well-known factor [4].

the same distribution, using the superposition of simulated functions $P_v(\tilde{E}_k)$ according to (1), yields $p_{v=0}(t \geq 3 \text{ s}) = (98.9 \pm 1.3)\%$. Similar results were obtained in the presence of the electron beam at cooling energy ($E_d = 0$) during storage. The CEI measurements unambiguously show that the ion beam is dominated by the vibrational ground state $v = 0$ after 3 s of storage, in consistency with the expected time scale of radiative thermalization, but both thermal and non-thermal vibrational distributions with a few percent of the ions in higher vibrational states are consistent with these data.

3.2. DR rate measurements

Absolute rates of electron-induced reactions yielding neutral products were obtained with an energy-sensitive surface barrier detector located behind the storage ring dipole magnet following the electron cooler. In particular, the rates of neutral fragment events with total masses of 3 amu (^3He), 4 amu (^4He) and 7 amu ($^3\text{He} + ^4\text{He}$) were observed as a function of E_d and time t after the injection, yielding the quantities $R_{(3)}(E_d;t)$, $R_{(4)}(E_d;t)$, and $R_{(7)}(E_d;t)$, respectively, and the rovibrationally averaged rate coefficient $\tilde{\alpha}_{\text{DR}}(E_d)$ is derived from these rates. Figure 1(a) shows the energy dependent DR rate coefficient $\tilde{\alpha}_{\text{DR}}(E_d)$ as obtained at 35–68 s after ion injection and corrected for the DR contributions from the toroid regions of the electron cooler [14]. The absolute rate coefficient was determined at an energy of $E_d = 7.3 \text{ eV}$ corresponding to the position of the broad resonance in figure 1(a) by considering the decay of the ion beam with and without the presence of the electron beam [4].

While only a weak time dependence of the DR rate is observed at higher energies beyond 0.1 eV, the low energy DR rate depends strongly on time. This is illustrated in figure 1(b), where the ratio $R_{(7)}(0;t)/R_{(3)}(0;t)$ is displayed versus time for two different electron densities. Between $\sim 5 \text{ s}$ and $\sim 30 \text{ s}$, the DR rate coefficient changes by almost a factor of 3. At long storage times an asymptotic ro-vibrationally averaged DR rate coefficient is reached; in the comparison of the two electron densities, a higher electron density leads to a faster approach to the asymptotic rate, while the final asymptotes are similar.

The observations in figure 1(b) clearly show that the DR reaction rate depends upon the rovibrational state of the interacting ions and that for a stored ion beam, the electron beam influences the rovibrational populations. By switching the electron beam off for different periods of time after the end of phase-space cooling (5 s), it was also seen that the value of $R_{(7)}(0;t)/R_{(3)}(0;t)$ at the moment when the electron beam

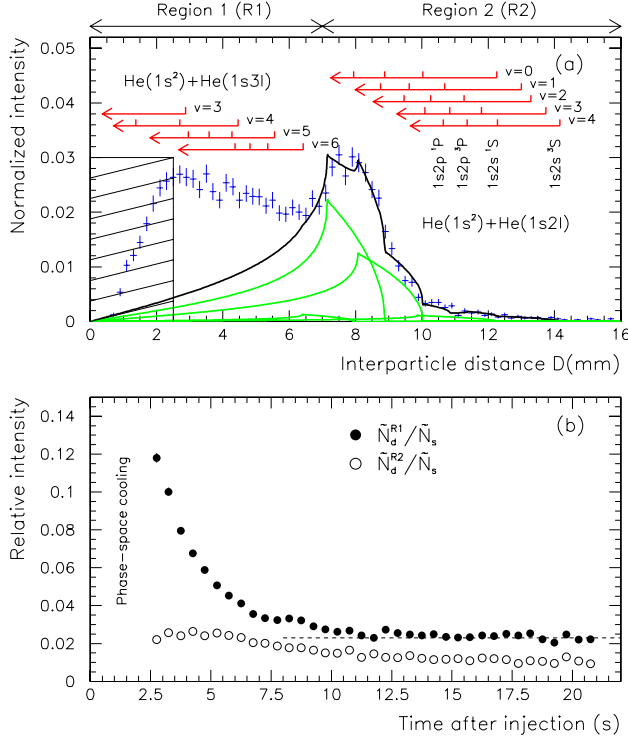


Figure 2. DR fragment imaging. (a) Distribution (crosses) of projected distances D as measured 10–22 s after ion injection. The vertical lines, grouped according to the initial v -levels, indicate the end points of the expected shapes $P_{v0m'l'}(D)$. The black curve shows a least-squares fit to the data (section 5.1) with gray lines indicating the included contributions with $v = 0$. The hatched area at low distance marks the region of limited detection due to overlapping spots on the imaging detector [4]. (b) Time evolution of the integrated signals in regions 1 and 2, \tilde{N}_d^{R1} and \tilde{N}_d^{R2} , after normalization to the detected number of one-body events, \tilde{N}_s .

is switched back on, decreases with longer periods of electrons off, demonstrating that the rovibrational population in the ion beam evolves over tens of seconds even if only radiative transitions and residual gas collisions occur.

Radiative transitions would drive the vibrational population of the stored ions to stabilize within a few seconds after injection, and the fast decay of the DR rate up to ~ 10 s could well represent the vibrational stabilization. That vibrational stabilization is observed for longer times with DR measurements than with the CEI technique (section 3.1) is expected, given the large DR cross sections for vibrationally excited levels as compared to $v = 0$ [3]. However, the slow evolution of the DR signal beyond 10 s must be attributed, based on its timescale, to changes in the *rotational* populations.

Overall, the results presented in this section demonstrate a significant contribution of rovibrationally excited levels to the measured low-energy DR rate coefficient, and hence the need to understand in more detail the rovibrational composition of the measured rate before quantitative information on DR can be extracted.

3.3. DR fragment imaging

The transverse coordinates of both fragments from individual DR events, identified by their arrival within a coincidence time window of a few microseconds, were recorded using the DR fragment imaging detector setup at the TSR [9]. For a DR reaction proceeding from a rovibrational level vJ to a final atomic channel nm' , the distribution of transverse (projected) interparticle distances (D) as obtained with this technique has a characteristic form $P_{vJnm'}(D)$ [10] that depends on the kinetic energy released. Contributions from various rotational levels cannot be directly resolved, and distinct features in the projected distance distribution are associated with individual vibrational levels and individual atomic quantum numbers. Using J -averaged DR rate coefficients $\tilde{\alpha}_{\text{DR}}^{vnm'}(0)$ and distance distributions $\tilde{P}_{vnm'}^{(T_{\text{rot}})}(D)$ for a suitable rotational temperature T_{rot} [9], the total spectrum of measured projected distances can be written as the superposition

$$P(D, t) = K(t) \sum_{vnm'} p_v(t) \tilde{\alpha}_{\text{DR}}^{vnm'}(0) \tilde{P}_{vnm'}^{(T_{\text{rot}})}(D), \quad (2)$$

where $K(t)$ is a normalization factor. The measured distributions of relative distances thus obtained reveal the relative contributions to the overall DR rate from different reaction channels vnm' , as characterized by $p_v(t)\tilde{\alpha}_{\text{DR}}^{vnm'}(0)$. For assigned vibrational levels v , these data also yield the branching ratios to the possible atomic final states.

The DR fragment imaging measurements were performed with an ion energy of $E_i = 3.36$ MeV and a detuning energy of $E_d = 0$. The projected distance distribution observed at 10–22 s is displayed (crosses) in figure 2(a). The spectrum in figure 2(a) has been divided in two parts with a border at $D \sim 7$ mm, namely region 1 and region 2 corresponding to transitions to the $n = 3$ and $n = 2$ final atomic states, respectively. For energetic reasons, zero-energy DR of ${}^3\text{He}^4\text{He}^+$ ions in $v \leq 2$ can only dissociate to the $n = 2$ final atomic states, associated with kinetic energy releases in excess of ~ 1 eV. On the contrary, for the vibrational levels $v \geq 3$ also the $n = 3$ final atomic states are accessible, however, associated with much smaller kinetic energy releases. In the observed projected distance distributions, contributions with end points at small D therefore indicate the presence of vibrationally excited ions in levels $v \geq 3$, and can *only* arise from such levels. Thus, the prominent contribution at low distances (region 1), arises from vibrationally excited ions in $v \geq 3$, while the peak structure at higher distances (region 2) cannot be immediately assigned to certain vibrational levels. The two regions shows different temporal evolutions as can be observed in figure 2(b); while the signal from region 1 initially decreases, the signal from region 2 shows a slight increase. From ~ 6.5 s onwards both signals decrease, the signal from region 1 essentially reaching a constant level after ~ 12 s, while that from region 2 continues to decrease slowly over the full observation period up to 22 s. The fact that the signals in region 1 and 2 have very different time structures for the first ~ 6.5 s proves that they originate from different parts of the rovibrational population in the ion beam at these times and indicates that the signal in region 2 arises from the lower vibrational levels ($v \leq 2$). Further arguments, given in section 4.1, allow us to conclude that the signal in region 2 mainly arises from $v = 0$. The time evolution on the longer time scale (≥ 10 s) can be unambiguously assigned to rotational states with different DR cross sections.

The data presented in figure 2 show that vibrational levels with $v \geq 3$ contribute significantly to the DR signal even after > 10 s of storage time, in sharp contrast to the expectation from radiative thermalization; this indeed proves that the stored ions experience vibrational excitation by some further mechanism(s).

4. Rovibrational excitation and cooling mechanisms

4.1. Pump-probe investigation of vibrational excitation

The observation that the signal in region 1 of figure 2(a) arises from higher vibrational states ($v \geq 3$) and that the major part of region 2 originates from DR of the lower vibrational states makes it possible to use a pump-probe type experiment to investigate the effect of the electron beam and of residual-gas collisions on the vibrational population.

For probing the effect of the electron beam, an experimental cycle was used for each injection in which the energy of the electron beam was altered in a regular time pattern. Several intervals of 1 s were spent at an excitation energy and were interrupted by probing intervals of 1 s, where projected fragment distance distributions were recorded at $E_d = 0$. The temporal variation of the signals from both regions after the end of excitation is shown for an excitation energy of 4 eV in figure 3(a). The DR signal from region 1 is enhanced right after the electron excitation period and then shows a significant, rapid decrease. Remarkably, no significant time variation is seen on the DR signal from region 2. This is a strong experimental evidence that the major part ($\geq 90\%$) of this signal originates from the vibrational ground state ($v = 0$), since the radiative lifetimes of all excited v levels are short enough that significant contributions to the DR signal in region 2 from such levels should reveal themselves by a decaying component. Similarly, excitation energies up to 10 eV were probed [figure 3(b)] and a clear variation of the excitation strength is seen for the signal in region 1, while no significant variation was seen in region 2.

To probe the effect of leaving the ${}^3\text{He}^4\text{He}^+$ ions under the influence of residual gas collisions only, a similar experimental cycle was used, but instead of stepping up the electron energy, the electron beam

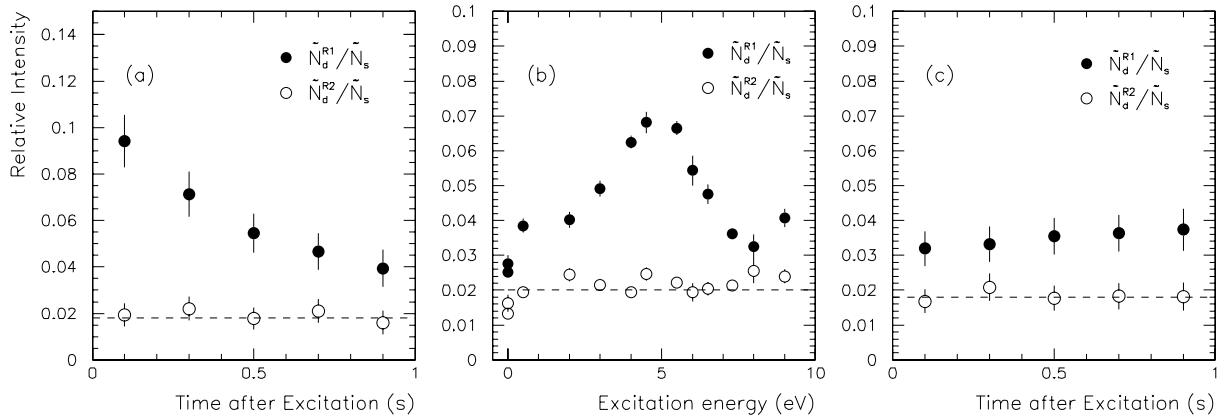


Figure 3. Pump-probe investigation of vibrational excitation, using the DR signals from region 1 ($v \geq 3$; filled circles) and region 2 (mainly $v = 0$; open circles) in the fragment imaging distribution. (a) Time scan following excitation with electrons at 4 eV. (b) Scan of electron excitation energy. (c) Time scan following off-periods of the electron cooler (see text). The counts were collected from the 4 probing periods for ≥ 9 s after injection; the counts in regions 1 and 2 have been normalized to the observed number \tilde{N}_s of one-body imaging events.

was turned off for 1 s between the probing periods. Figure 3(c) shows that under these conditions the probe signal from region 1 is essentially constant, possibly with a slight temporal increase showing the effect of vibrational excitation from the toroid regions after the electrons have been switched back on. The signal ratio between regions 1 and 2 during the probing period continuously stays at ~ 2 , a value close to that found when the electron beam was continuously on [$t > 9$ s in figure 1(b)]. Thus, the dominant part of the observed vibrational excitation persists in the stored ${}^3\text{He}^4\text{He}^+$ beam even during the absence of the electron beam for a time that exceeds the radiative lifetime of the excited vibrational levels, and we conclude that ion collisions with the residual gas play the dominant role in maintaining a non-thermal vibrational population in the stored ion beam.

4.2. Electron induced rotational cooling

Two possible effects must be considered to explain the electron induced evolution of the rotational distribution as reported in section 3.2, namely preferential depletion of J levels by the DR reaction, or inelastic electron-impact excitation and de-excitation (see, e.g., [15]). Preferential depletion by the DR reaction would require a significant contribution of the DR rate-constant to the beam decay rate, which was not observed in the measurements. Thus, the electron induced rate variation seen in figure 1(b) occurs over a time scale of ~ 10 s; therefore with the applied electron density of $n_e = 1.2 \times 10^7 \text{ cm}^{-3}$, the rate coefficients involved in the underlying changes of the rotational level populations should have a size of $\sim (10 \text{ s} \cdot \eta n_e)^{-1} = 3 \times 10^{-7} \text{ cm}^3/\text{s}$ ($\eta = 0.027$ being the length of the electron cooler relative to the TSR circumference). On the other hand, the observed absolute DR rate coefficient at $E_d = 0$ (including contributions from excited states with $v \geq 3$) amounts to only $\sim 3 \times 10^{-9} \text{ cm}^3/\text{s}$, much smaller than required to depopulate a significant part of the ion beam. These arguments leave inelastic electron-induced cooling as the mechanism driving the evolution of the rotational states in the stored ion beam.

5. Results on DR from the vibrational ground state

5.1. Final state branching at near-zero energy

According to the pump-probe measurements, at most $\sim 10\%$ of the signal in region 2 ($D > 7$ mm) of the DR fragment imaging distribution at $E_d = 0$ can arise from ${}^3\text{He}^4\text{He}^+$ ions in the vibrationally excited states. Therefore, the dominant signal contributions in this region were assigned to DR into different final atomic states from the vibrational ground state, and the respective signal contributions were obtained by

Table 1. Measured final state branching ratios following low-energy DR from the $v = 0$ level of ${}^3\text{He}^4\text{He}^+$.

Final channel	Branching ratio (%)
$\text{He}(1s^2{}^1S) + \text{He}(1s2s^3S)$	3.7 ± 1.2
$\text{He}(1s^2{}^1S) + \text{He}(1s2s^1S)$	37.4 ± 4.0
$\text{He}(1s^2{}^1S) + \text{He}(1s2p^3P)$	58.6 ± 5.2
$\text{He}(1s^2{}^1S) + \text{He}(1s2p^1P)$	2.9 ± 3.0

fitting to the data a corresponding superposition of signals [cf. (2)]; this yields the full line in figure 2(a). Contributions to the distribution whose shape cannot be attributed to $v = 0$ ions are on the few-percent level; with the remaining arbitrariness caused by the similarity of the energy release for the different channels with $v \neq 0$, they were fitted to certain final states reached from ions with $v = 3$ and 4 [4]. Table 1 lists the branching ratio obtained from the fit for the vibrational ground state, showing a dominance of the $1s2p^3P$ and $1s2s^1S$ fine structure levels. The levels $v \geq 3$ do yield a substantial DR signal in region 1 ($n \geq 3$ final atomic states) but, as seen in section 4.1 contribute very little to region 2. Hence, we find ions in these levels to have a strong preference for DR into the higher-lying atomic states, avoiding the $n = 2$ final levels.

5.2. Absolute rate coefficient

An absolute rate coefficient of $\tilde{\alpha}_{\text{DR}}(E_r) = 2.8(4) \times 10^{-8} \text{ cm}^3/\text{s}$ was measured at $E_r = 7.3 \text{ eV}$. The energy-dependent rate coefficient measurements shown in figure 1(a) were normalized using this absolute rate, thus giving a zero-energy toroid corrected DR rate coefficient of $\tilde{\alpha}_{\text{DR}}(0) = 2.7(4) \times 10^{-9} \text{ cm}^3/\text{s}$ for $t > 35 \text{ s}$. As seen from the fragment imaging measurements (section 3.3), this rate coefficient has a significant contribution from higher vibrational levels. With the assignment and the fit of the DR fragment imaging distribution [figure 2(a)] the fraction of the observed DR rate at $E_d = 0$ that originates from $v = 0$ in this spectrum can be determined to be $\tilde{I}(v = 0) = 0.54(5)$. However, the total intensity in the fragment imaging spectrum, corresponding to the toroid-corrected rate coefficient $\tilde{\alpha}_{\text{DR}}(0)$, is reduced by the limited detection at small distances. By a comparison of the toroid contributions as obtained by the DR fragment imaging and the DR rate coefficient measurements this reduction factor can indeed be determined [4] as $(1 - \tilde{f}_d)$, where $\tilde{f}_d = 0.49(11)$. The DR rate coefficient from the vibrational ground state can then be deduced as $(1 - \tilde{f}_d) \times \tilde{I}(v = 0) \times \tilde{\alpha}_{\text{DR}}(0)$, yielding

$$\alpha_{\text{DR}}^{v=0}(0) = (7.3 \pm 2.1) \times 10^{-10} \text{ cm}^3/\text{s}. \quad (3)$$

This rate coefficient still represents an average over the relaxed rotational distribution resulting after storage and electron cooling for 35 s. Assuming a DR cross section varying as $\propto E^{-1}$ up to $\sim 0.1 \text{ eV}$, the merged-beams rate coefficient $\alpha_{\text{DR}}^{v=0}(0)$ can be converted to a rate coefficient for a thermal, isotropic electron velocity distribution at 300 K by the division by a factor of 2.2, yielding $\alpha_{T,\text{DR}}^{v=0} = (3.3 \pm 0.9) \times 10^{-10} \text{ cm}^3/\text{s}$.

The energy dependent rate coefficient [figure 1(a)] displays a broad peak at 3–12 eV shown in detail in figure 4(a). The position and the width of this structure matches well the energies of vertical transitions from the ionic vibrational ground state to dissociating neutral Rydberg states which converge to the repulsive $A^2\Sigma_g^+$ ionic state. Recently, Royal and Orel [16] have obtained results for the high-energy DR of ${}^3\text{He}^4\text{He}^+$ ($\sim 2\text{--}13 \text{ eV}$). Their peak cross section of $0.75 \times 10^{-17} \text{ cm}^2$ is significantly smaller than our result. While the peak position is in good agreement, the calculated peak shape does not reproduce the asymmetry found in our data for $t > 35 \text{ s}$.

Figure 4(b) shows the measured rate coefficient at the highest energies. Several structures are clearly seen: A narrow peak at $\sim 19 \text{ eV}$, a large broad peak at $\sim 22.5 \text{ eV}$, a plateau-like behavior at 25–27 eV, and a small modulation at 31 eV before the rate declines. In this region of energy, vertical transitions from the

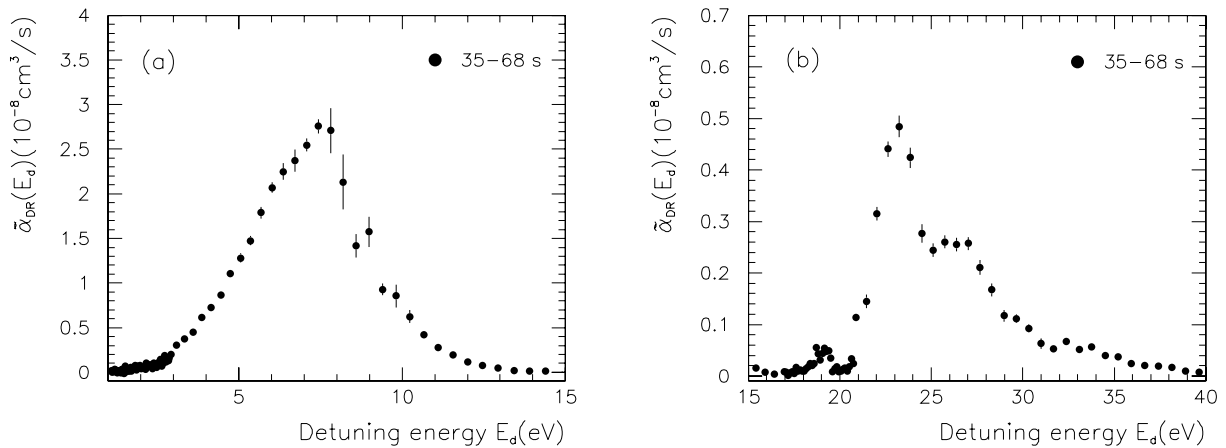


Figure 4. Detailed view of the measured toroid corrected rate coefficients at high energies obtained at 35–68 s. (a) Broad peak due to DR through the Rydberg series converging to the $A^2\Sigma_g^+$ ionic state. (b) Structures resulting from DR through Rydberg states associated with ionic states that correlates to the $\text{He}^+(1s) + \text{He}(1s2l)$ atomic limits.

ionic vibrational ground state can reach dissociating neutral Rydberg states converging to highly excited states of the He_2^+ ion, in particular the ionic curves correlated to the $\text{He}^+(1s) + \text{He}(1s2l)$ atomic limits. The very detailed structure (with the narrow peak at ~ 19 eV) may indicate that certain core-excited Rydberg states play a dominant role in the DR at these energies.

6. Conclusion

This study of $^3\text{He}^4\text{He}^+$ with the storage ring technique has given a qualitative understanding of the evolution of rovibrational populations of a stored ion beam and quantitative results on the DR from the ground state of the helium dimer ion. The vibrationally hot population of the ensemble of $^3\text{He}^4\text{He}^+$ injected into TSR is being cooled by radiative transitions towards room temperature and being heated by residual gas collisions and energetic electron-ion collisions, resulting in a non-thermal equilibrium. The rotational population is cooled both by radiative transitions and by low energy electron ion collisions, resulting in an equilibrium presumably below room temperature. For the vibrational ground state, the DR rate coefficient (section 5.2) and the branching ratios to final atomic channels as listed in table 1 were determined. The energy dependent rate coefficient displays several pronounced structures, in particular a broad peak at 3–12 eV, a narrow peak at ~ 19 eV, a large broad peak at ~ 22.5 eV, and a plateau-like behavior at 25–27 eV. Similar experiments on $^4\text{He}_2^+$ are under analysis; they also show considerable effects of electron-induced ro-vibrational de-excitation of the stored ions.

Acknowledgments

This work has been funded by the German Israel Foundation for Scientific Research (GIF) under Contract No. I-707-55.7/2001 and by the European Community within the Research Training Network “Electron Transfer Reactions”. HBP acknowledges support from the European Community program IHP through a Marie Curie fellowship under contract No. HPMF-CT-2002-01833.

References

- [1] Stancil PC, Lepp S and Dalgarno A 1998 *Astrophys. J* **509** 1
- [2] Deloche R *et al.* 1976 *Phys. Rev. A* **13** 1140
- [3] Carata L, Orel AE and Suzor-Weiner A 1999 *Phys. Rev. A* **59** 2804
- [4] Pedersen HB *et al.* 2004 *Phys. Rev. A* (submitted)

- [5] Buhr H *et al.* (to be published)
- [6] Steck M *et al.* 1990 *Nucl. Instrum. Methods Phys. Res. A* **287** 324
- [7] Pastuszka S *et al.* 1996 *Nucl. Instrum. Methods Phys. Res. A* **369** 11
- [8] Kilgus G, Habs D, Schwalm D, Wolf A, Badnell NR and Müller A 1992 *Phys. Rev. A* **46** 5730
- [9] Amitay Z *et al.* 1999 *Phys. Rev. A* **60** 3769
- [10] Amitay Z *et al.* 1996 *Phys. Rev. A* **54** 4032
- [11] Wester R *et al.* 1998 *Nucl. Instrum. Methods Phys. Res. A* **413** 379
- [12] Al-Khalili A *et al.* 2003 *Phys. Rev. A* **68** 042702
- [13] Lammich L *et al.* 2004 *Phys. Rev. A* **69** 062904
- [14] Lampert A, Wolf A, Habs D, Kenntner J, Kilgus G, Schwalm D, Pinzola M S and Badnell NR 1996 *Phys. Rev. A* **53** 1413
- [15] Rabadan I, Sarpal S K and Tennyson J 1998 *Mon. Not. R. Astron.* **299** 171
- [16] Royal J and Orel A E 2005 *J. Phys.: Conf. Series* this volume